

STRATEGIES FOR ELECTRON PAIR RECONSTRUCTION IN CBM

T.Galatyuk¹, J.Stroth²

¹Gesellschaft für Schwerionenforschung mbH, Darmstadt, Germany
²Institut für Kernphysik, Frankfurt, Germany

Abstract

In this paper, strategies to reduce the combinatorial background in electron pair measurements with the Compressed Baryonic Matter (CBM) detector are discussed. The main goal is to study the feasibility to effectively reduce the combinatorial background with the currently foreseen experimental setup, which does not provide electron identification in front of the magnetic field. The collision system investigated is $Au + Au$ at 25 AGeV. Throughout this study, we assume perfect track reconstruction and particle identification.

1 Introduction

The study of the electromagnetic structure of hadrons plays an important role in understanding the nature of matter. In particular the emission of lepton pairs out of the hot and dense collision zone of heavy ion reactions is a promising probe to investigate the in-medium properties of hadrons and in general the properties of matter under such extreme conditions. Recent experimental results of the CERES [1] and the NA60 [2] collaborations show an enhancement in the invariant mass region $0.3 \div 0.7 \text{ GeV}/c^2$, in principle similar to the first one, observed by the DLS [3] collaboration. First results of the HADES [4] collaboration show a moderate enhancement above η -Dalitz contributions for C+C at 2 AGeV. There are several theoretical explanations of this observation, most of them focusing on possible in-medium modifications of the properties of vector mesons. Phenomenologically, the in-medium effects associated with the intermediate ρ can be classified according to the following extreme scenarios:

- In-medium "dropping" ρ mass (a la Brown and Rho [5]);
- In-medium "broadening" ρ mass (e.g. Rapp, Wambach et al. [6]).

It is currently debated to which extend these effects are independent of each other and whether they are more driven by baryonic density or by temperature (i.e. pion density). The CBM experiment will explore the region in the phase diagram of moderate temperatures and high baryonic densities. The experimental task of the CBM is to identify both hadrons and leptons and to detect rare probes out of the reaction zone formed in central heavy ion collision. An essential issue in the experimental strategy to assess the low-mass vector mesons by means of their electromagnetic decay is whether electron or muons are the best choice. Whereas electron pairs do not impose phase space limitations accessing the very low mass region of the pair mass spectrum, muons on the other hand are generally preferable because of a beneficial background situation. The purity and efficiency of lepton identification for both electrons or muons and for a given experimental set-up will have a large impact on the physics performance.

A detailed description of the experimental setup is given in [7]. For the present analysis an *Active Shielding Magnetic Field* for bending the charged particle trajectories was used. The acceptances of the Silicon Tracker System (STS), Ring Imaging Cherenkov detector (RICH) and Transition Radiation Detectors (TRD) were taken into account, however, no track reconstruction or particles identification algorithms were used. The main difference of CBM compared to other experiments is that there is no hadron blind detector in front of the tracking system.

2 Input to the simulation

2.1 Event generator

The simulations were performed for the collision system $Au + Au$ at a beam momentum of 25 AGeV. The final state phase space distributions of hadrons and photons were generated using the relativistic transport code UrQMD [8]. The simulation was done for zero impact parameter (central collision). The phase space distributions of electrons and positrons from purely leptonic and semi-leptonic (i.e. Dalitz) decays of light vector mesons (ρ^0 , ω , ϕ) were obtained using the PLUTO [9] event generator. To enhance the statistics for these rare decays one decay of a vector meson was embedded in each UrQMD event. In the analysis, contributions from these enhanced sources were normalized according to their mean multiplicities as predicted by the

Hadron-String Dynamics [10] model and the branching ratios. The mean multiplicities, decay channels and branching ratios of background and signal lepton sources are presented in Table 1. On average, there is one leptonic decay of light vector mesons (excluding η -Dalitz) in 400 central $Au + Au$ collisions at 25 AGeV.

particle	N/event	decay channel	BR
π^0	365	$e^+e^-\gamma$	1.198×10^{-2}
η	36	$e^+e^-\gamma$	5.0×10^{-3}
ω	38	$e^+e^-\pi^0$	5.9×10^{-4}
		e^+e^-	7.07×10^{-5}
ρ^0	23	e^+e^-	4.44×10^{-5}
ϕ	1.28	e^+e^-	3.09×10^{-4}

Table 1: Mean meson multiplicities, their dominant leptonic decay channels and branching ratios for central $Au + Au$ collisions at 25 AGeV

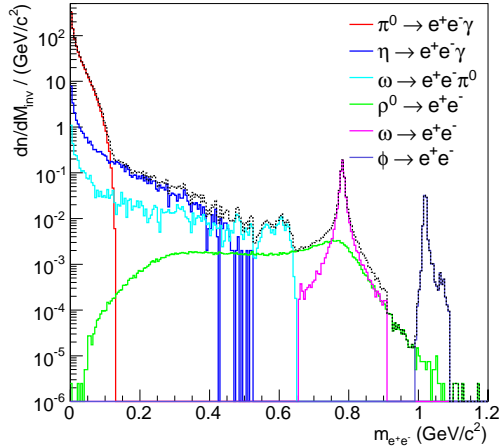


Figure 1: Invariant mass distribution for central $Au + Au$ collisions at 25 AGeV (full phase space). Red: π^0 -Dalitz decay; dark blue: η -Dalitz decay; blue: ω -Dalitz decay; green: ρ^0 , magenta: ω , violet: ϕ direct dilepton decay. The black line shows the sum of all contributions.

In Figure 1 the cocktail of electron pair sources is shown for central $Au + Au$ collisions at 25 AGeV as it was used as input to the simulation. The spectrum shown is integrated over the full phase space. The ρ meson mass distribution is generated by including a Breit-Wigner shape around the pole mass, thermal phase space factors, and a factor $1/M^3$ to account for vector dominance in the decay into e^+e^- . All particles were finally propagated through the detector system with the simulation tool Cbmroot2 using the GEANT3 [11] package. We used the standard geometry [12]. A single 25 μm gold target was assumed.

2.2 Modification to the spectrometer set-up

To increase the acceptance for low momentum particles the magnetic field was reduced to $B_{max} = 0.33$ T. Substantial reconstruction capability for low-momentum tracks is essential for identifying electron pairs from γ conversion and Dalitz decay of π^0 , as the topology of these processes has a relevant fraction where tracks with moderate laboratory momentum are accompanied by very soft tracks which are rapidly bend out of the acceptance of the tracking station (see Figure 2). A second important requirement for efficient back-

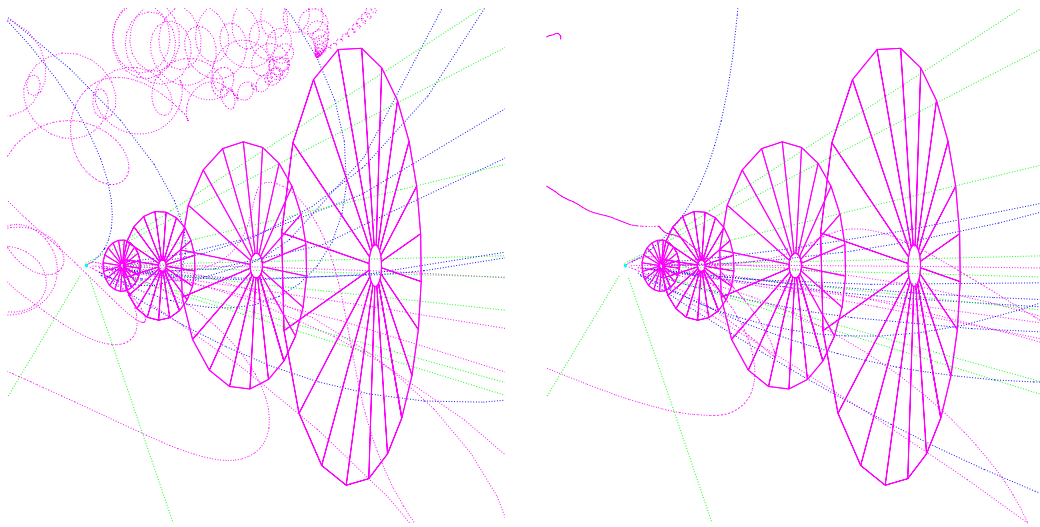


Figure 2: Trajectories of γ (green), e^+ (magenta), e^- (blue) from π^0 -Dalitz decay. Left panel: $B_{max} = 1.1$ T, right panel: $B_{max} = 0.33$ T.

ground rejection is to enable an opening angle measurement even for pairs where one of the tracks is not fully reconstructed. To improve in this respect, the magnetic field was shifted 20 cm downstream. This further reduces the magnetic field strength between target and first tracking station by a factor of 2. However, this action at the same time reduces the momentum resolution considerably. The final configuration will result from trading background rejection capability against invariant mass resolution. A final conclusion on the appropriate strategy, however, cannot be drawn at this level of investigation. The field configuration used for the simulation is depicted in Figure 3 (right panel).

2.3 Data analysis

For the investigation presented here a simplified analysis was used. A track was considered fully reconstructed if tracking stations 2 to 7 were traversed

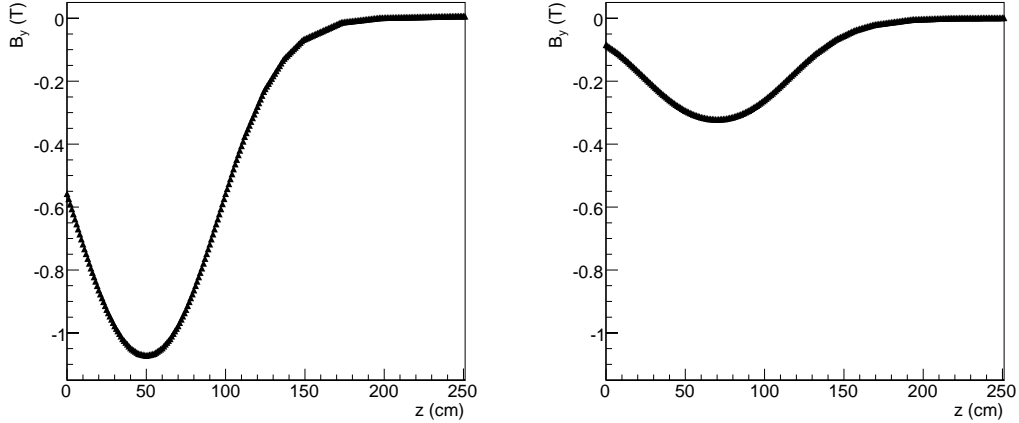


Figure 3: Vertical magnetic field strength (i.e. B_y) along the beam axis. Left panel: standard configuration. Right panel: reduced field, shifted 20 cm downstream.

by the particle and the RICH detector as well as the 3 TRD detectors were hit. The first STS station, which is placed at 5 cm downstream from the target, was not used in the analysis due to its limited acceptance for tracks with small laboratory polar angles (i.e. due to its large inner hole, in the following discussion we will refer to the second STS station as "first STS"). Perfect particle identification was assumed for fully reconstructed tracks. For these tracks, the Monte-Carlo momentum was used for the physics analysis. The reconstruction and detector efficiency was taken to be unity. Moreover, tracks were considered partially reconstructed if at least 4 STS stations were traversed. For these tracks only the charge sign information and the Monte-Carlo momentum were used in the analysis. In the following we refer to *Full Track* and *Track Segment* in case of fully reconstructed and partially reconstructed tracks, respectively. In all cases the Monte-Carlo momenta were smeared assuming 1 % momentum resolution independent of particle momentum.

Figure 4 shows the transverse momentum versus rapidity of accepted electron pairs from π^0 (main background source) and ρ^0 meson decay, i.e. for $\pi \rightarrow \gamma e^+ e^-$ and $\rho^0 \rightarrow e^+ e^-$. Please note that the majority of pairs from pion decay appears at low or moderate transverse momentum.

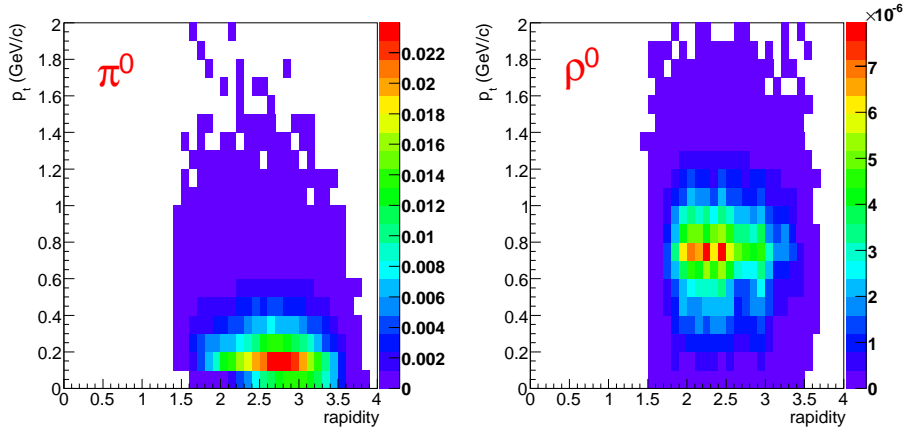


Figure 4: Transverse momentum versus rapidity distribution for π^0 -Dalitz decay (left panel) and for ρ^0 (right panel)

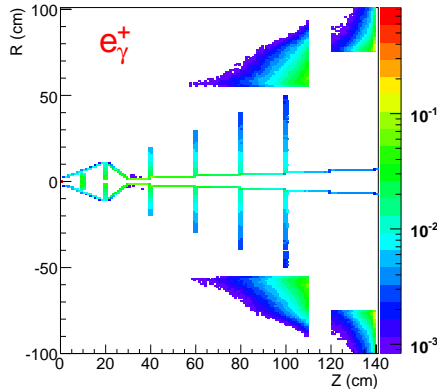


Figure 5: Radial vs. longitudinal distribution of emission sites for positrons created through γ conversion. Contributions come from the target, the tracking stations, the beam pipe and the magnet yoke.

3 Characteristics of the background

The dominant background sources are random combinations of electrons and positrons from π^0 -Dalitz decay and γ conversion. In a central $Au + Au$ collision about 360 π^0 mesons are produced, which subsequently decay into $e^+e^-\gamma$ ($\Gamma/\Gamma_{tot} = 0.012$) and to 2γ ($\Gamma/\Gamma_{tot} = 0.988$). Although most of the photons from π^0 decay are converted outside the acceptance of the tracking station, a substantial background arises from conversion in the target (see Figure 5). A characteristic feature of conversion and Dalitz decays is the moderate decay momentum of the electron pair. This generally leads to small opening angles and comparatively small laboratory momenta. Consequently, in many cases one soft partner traverses only one or up to three STS stations and can hence not be reconstructed, as it is shown in Figure 6. For that

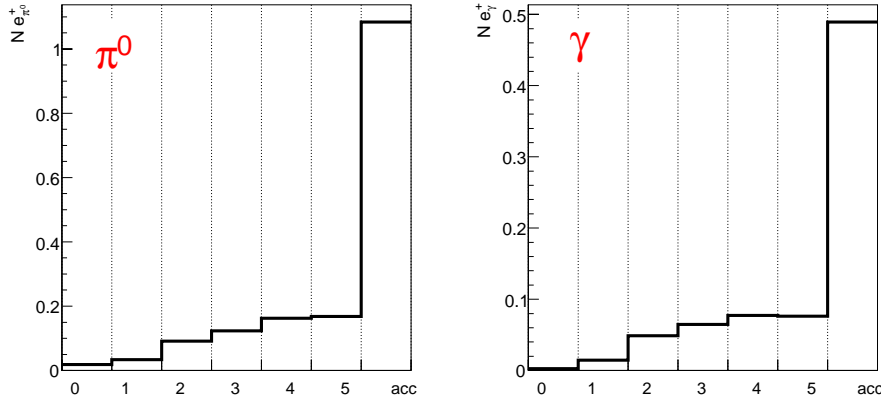


Figure 6: Number of STS stations traversed by e^+ from π^0 -Dalitz decay and γ conversion. Only cases are shown where the partner electron was fully reconstructed.

reason all tracks were categorized in the following way:

Track Fragment: tracks with less than 4 STS hits (points)

$$(N_{TrackFragment}^{\pi} = 0.27, N_{TrackFragment}^{\gamma} = 0.13);$$

Track Segment: tracks with a minimum of 4 STS hits (points)

$$(N_{TrackSegment}^{\pi} = 0.33, N_{TrackSegment}^{\gamma} = 0.15);$$

Full Track: tracks identified as electrons - 6 STS points, a RICH point and three TRD points ($N_{acc}^{\pi} = 1.08, N_{acc}^{\gamma} = 0.49$).

On the Track Fragment and Track Segment level all charged particles (≈ 700 in the geometrical acceptance) are included in the analysis. Despite their particular decay pattern, a large number of electron pairs from γ conversion are fully tracked (see Figure 6). Such pairs are quite unique in as much as they combine to very small invariant masses, so they are best removed before the other background rejection methods are applied to the electron and positron tracks.

4 Rejection strategy

The central problem of the analysis is to recognize and reject as many as possible of the partially reconstructed leptons from γ conversion and π^0 -Dalitz decays. On the other hand, we are not interested to cut substantially π^0 -Dalitz decay for better comparison to theory and to check normalization.

In contrast to other electron pair spectrometers (e.g. DLS, HADES, CERES) in CBM there is no detector system which can provide PID information in front of the magnetic field. That means that all close pairs are "opened" by the magnetic field before the electrons will reach the RICH detector. Hence, the rejection strategy has to rely to a large extent on the track topology of pairs in the silicon tracking station. It is the main purpose of this work to study the respective performance of CBM, in particular of the STS, in the given geometry and to indicate directions for possible modifications of the spectrometer design in order to improve it further.

The strategy of background rejection comprises three steps. The first step is to identify and reject true pairs originating from conversion, the second step is to remove single tracks where the true partner was not fully reconstructed, the third step is to assign pairs with a characteristic pattern to π^0 -Dalitz pairs which then are filled to the histograms but not used for combinatorics. The group of tracks used are fully identified electron or positron tracks; fake tracks or misidentified charged pion tracks are not considered here but will be subject to a more advanced simulation.

At this stage of the analysis, the cuts to be described in the following sections are not optimised in a strict sense, i.e. by maximising the significance in the final invariant mass spectrum. Instead, reasonable cut values are chosen by comparing the signal to the main background source. The cut values will most probably change once a realistic detector response is taken into account.

4.1 Conversion pair cut

From the right panel in Figure 6 it can be seen that 50% of the electron pairs originating from conversion in the target are fully reconstructed. Conversion pairs have very small invariant masses and are thus essentially located below $25 \text{ MeV}/c^2$. We assume, that all reconstructed pairs which have an invariant mass smaller than $25 \text{ MeV}/c^2$ stem from photon conversion. Tracks forming such pairs are fully removed from the sample in this first step.

4.2 Single track cuts

4.2.1 Close neighbor cut

An important characteristic of conversion is the small opening angle and since the magnetic field in first STS station is small, the distance between the partners remains small up to the first station. To reject the remaining track of such a pair in cases where the partner track was not even reconstructed

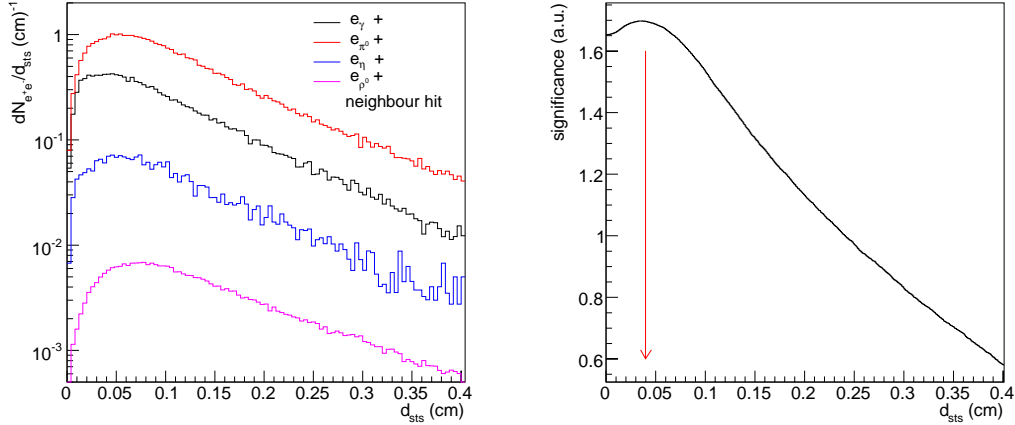


Figure 7: (Left panel) Distance to nearest neighbor hit in the 1st STS station. Red: full e_{π^0} + closest hit; black: e_{γ} + closest hit; blue: e_{η} + closest hit; magenta: e_{ρ^0} + closest hit, scaled by factor 10. (Right panel) Significance (see text) as a function of the cut value. The arrow marks the value in the cut variable where the significance is maximal.

as a Track Segment we inspect the vicinity of the Full Track in the first STS station in order to find the hit of the partner. Figure 7 shows the distance between the intersection point of an electron track in the first STS station to its nearest neighbor hit (d_{STS}) for different sources of lepton tracks. Since no particle ID nor even a charge sign can be assigned to this next neighbor hit all charged particles can potentially appear as fake partners. Hence, in particular in the region of highest track density, a cut on d_{STS} can substantially remove signal tracks, i.e. one of the tracks from an open pair.

To find the optimum, the cut was placed such that $S/\sqrt{S+B}$ is maximized. Here S is the number of electron tracks from ρ^0 + neighbor hit and B the number of electron tracks from γ conversion + neighbor hit, each surviving the cut. We remove tracks if d_{STS} is below 0.45 mm.

4.2.2 Transverse momentum of closest neighbor track segment

As can be seen from Figure 7 still a large fraction of conversion tracks survive the cut described before. In the next step we try to identify true partners of background tracks (which survive the cut on d_{STS}) in the class of Track Segments. We use information about the transverse momentum of Track Segments. Figure 8 shows the transverse momentum distribution of closest Track Segments for different sources of a fully reconstructed lepton tracks. The cut on this observable is optimized by maximizing $S/\sqrt{S+B}$, where S

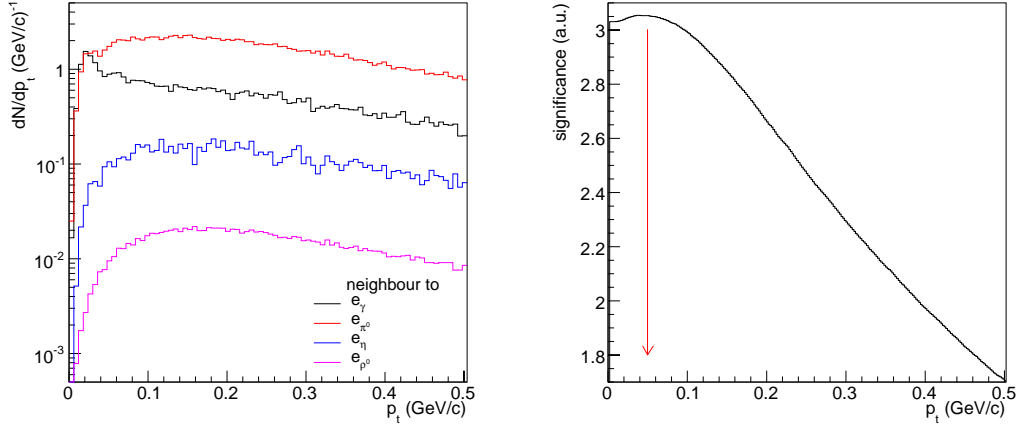


Figure 8: (Left panel) Transverse momentum of the neighbor Track Segment. Red: e_{π^0} + closest Track Segment, black: e_{γ} + closest Track Segment; blue: e_{η} + closest Track Segment; magenta: e_{ρ^0} + closest track segment scaled by factor 10. (Right panel) Significance (see text) as a function of the cut value. The arrow marks the value in the cut variable where the significance is maximal. The figure shows the distribution after previous cuts.

is the number of electron tracks from ρ^0 with a close Track Segment and B the number of electron tracks from π^0 -Dalitz decay, also with a close Track Segment. If the transverse momentum of the partner track segment is below 50 MeV/c, fully reconstructed track and Track Segment are rejected. It is clear that this cut will mostly remove combinations between a Full Track from γ conversion and its closest Track Segment. By optimizing cut using as B π^0 -Dalitz combination we cut (π^0 + closest Track Segment) and at the same time (γ + closest Track Segment) combinations.

4.2.3 Correlation of opening angle and invariant mass of closest neighbor Track Segment

Figure 9 shows the opening angle vs. invariant mass distribution. The pair invariant mass was calculated assuming $m_{Track\ Segment} = m_{e^-}$. A wedge cut is used to reject background. The ratio (number of combinations in the cut region/ total number of combinations) for different cases (signal electron track(ρ^0) + closest neighbor, background track (π^0 or γ) + closest neighbor) were calculated (see Figure 10). As optimum value was taken $\theta_{1,2} = 5^\circ$ and $m_{e^-e^+} = 0.1$ GeV/c². If $\theta_{1,2}$ and $m_{e^-e^+}$ of Full Track and closest Track Segment corresponds to the cut region, the Full Track and the Track Segment are rejected.

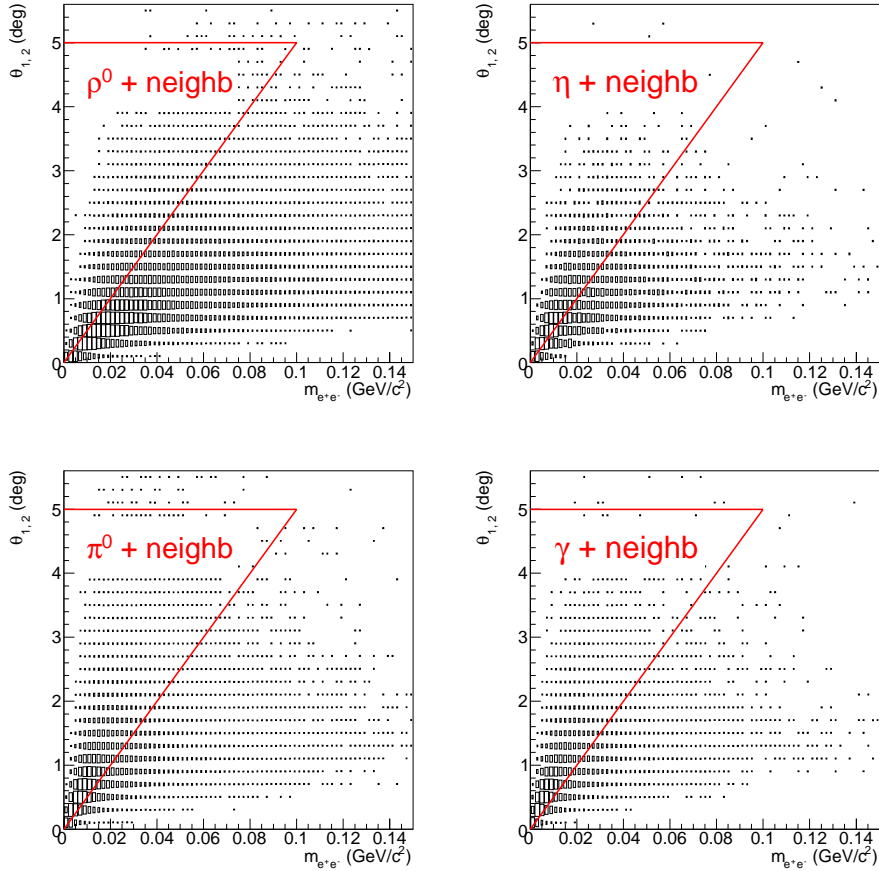


Figure 9: Opening angle vs. invariant mass for combinations of a Full Track with a next neighbor Track Segment. For the track segment the rest mass of an electron is assumed. The distribution is separately shown for cases where the Full Track stems from ρ^0 , η , π^0 decay and photon conversion, γ , respectively. The red lines denote the cut wedge. Tracks belonging to a pair inside the triangle are rejected. The figure shows the distribution after previous cuts.

4.2.4 Transverse momentum of identified leptons

Finally we exploit the transverse momentum of fully reconstructed tracks. Again, due to the small decay momentum and the strong exponential fall-off of the pion center-of-mass momentum spectrum the lepton tracks from the background sources are predominantly at low p_t . On the other hand, it is expected that radiation out of the dense phase of the collision also appears at low or moderate transverse momentum: pion-pion fusion, being the dominant process for populating ρ -like states in a hot pion gas, will favor strength located at low invariant mass and at moderate momentum. Figure 12 shows

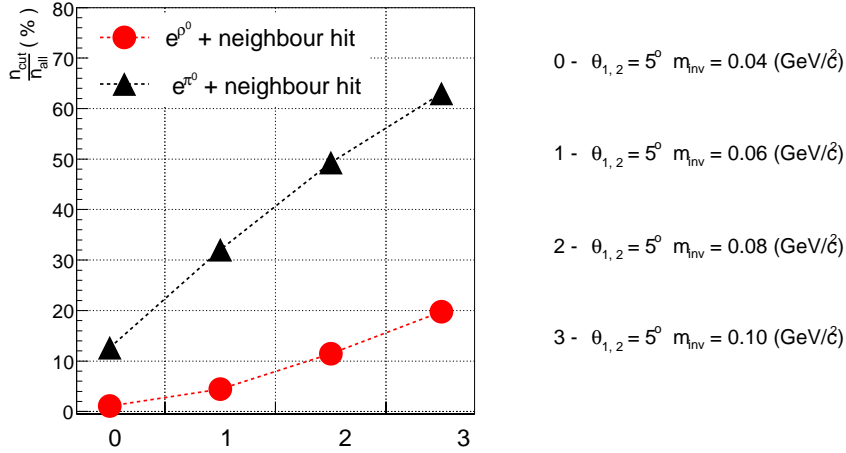


Figure 10: Performance of the rejection cut exploiting the opening angle – invariant mass correlation of a fully reconstructed track with its closest Track Segment. Case 3 was taken (20% of (signal electron track + neighbor hit) (red points) combinations and at the same time 63% of (background electron track + neighbor hit) (black triangle) combinations are rejected).

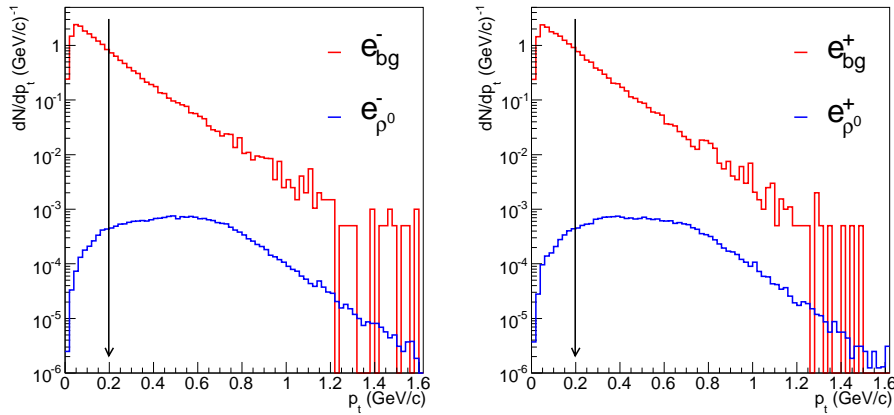


Figure 11: Transverse momentum distribution. Red: leptons from background sources, blue: leptons from signal. The arrow indicates the cut value. The figure shows the distribution after previous cuts.

that exactly in this region medium effects might enhance the strength of ρ -meson like states. A comparatively high transverse momentum cut-off will exclude a substantial part of the phase space where the modification of the ρ meson spectral function is most prominent. Figure 11 shows transverse momentum distributions of fully reconstructed tracks. By removing tracks

with $p_t \leq 200$ MeV/c one significantly lowers the combinatorial background but at the expense that an interesting region of the phase space would not be observed. Moreover, such a cut essentially removes all contributions to the signal invariant mass spectrum originating from π^0 decay.

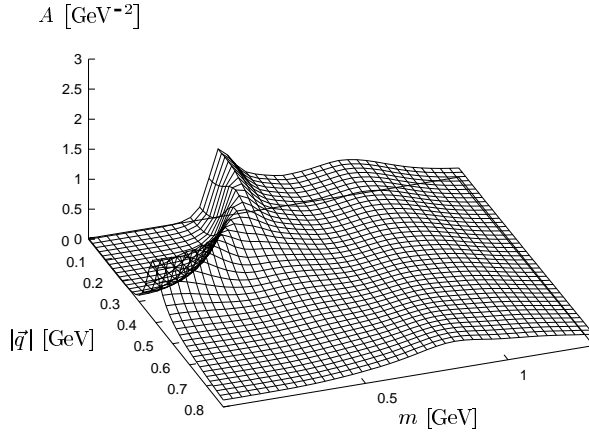


Figure 12: Self-consistent averaged spectral function of the ρ^0 meson for $\rho_N = 2 \rho_0$ [13]

4.3 Pair cuts

4.4 Opening angle cut

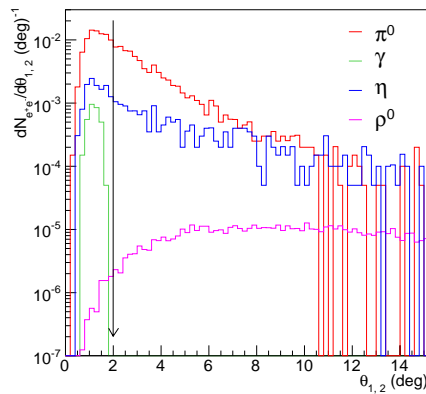


Figure 13: Opening angle distribution for electron pairs from π^0 -Dalitz decay (red), γ conversion (green), η -Dalitz decay (blue) and ρ^0 decay (magenta). The arrow indicates the cut value. The figure shows the distribution after previous cuts.

The main interest of low-mass pair spectroscopy is to reconstruct ρ^0, ω and ϕ mesons. In case these vector mesons decay exclusively into a pair of electrons, the rest mass of the meson is fully transformed into decay momentum. Hence these pairs will generally appear with a considerable opening angle. In contrast, pairs from photo conversion and also from Dalitz decays

of light mesons feature small opening angles. Figure 13 shows opening angle distributions for a number of different sources. Note the strong rise towards small opening angles for all but the exclusive vector meson decays. In the analysis Full Tracks forming pairs with an opening angle ($\theta_{1,2} \leq 2^\circ$) are removed.

4.4.1 Dalitz decay reconstruction

Finally, pairs with an invariant mass below 200 MeV/c² are assumed to origin from π^0 -Dalitz decays. The respective invariant mass is filled to the histogram but the corresponding tracks are not further used to form other pairs. All cuts established for background rejection are summarized in Table 2.

	cut	optimum value
	small invariant mass cut	0.025 GeV/c ²
	closest neighbor hits cut	0.045 cm
	p_t of closest neighbor Track Segment cut	0.05 GeV/c
	$(\theta_{1,2} + m_{e^-e^+})$ of closest neighbor Track Segment cut	$5^\circ + 0.01$ GeV/c ²
	p_t of identified leptons cut	0.2 GeV/c
	opening angle cut	2°
	Dalitz decay reconstruction	0.2 GeV/c ²

Table 2: Optimized cut values

5 Results

The invariant mass spectrum arising after applying all cuts described above is shown in Figure 14 (right panel). For comparison, the respective contribution before background rejection is shown in the left panel. Note that the analysis procedure does not introduce severe phase space limitations for the reconstruction of vector mesons (Figure 15, see also Figure 4). The reconstructed pions, however, predominantly appear at higher p_t . For clarity, the cut efficiency is shown in Figure 16 separately for each analysis step and for three different invariant mass regions:

- $0 < m_{e^+e^-}/(\text{GeV}/c^2) < 0.2$ - π^0 -Dalitz;
- $0.2 < m_{e^+e^-}/(\text{GeV}/c^2) < 0.6$ - enhancement region;
- $0.6 < m_{e^+e^-}/(\text{GeV}/c^2) < 0.9$ - ω , ϕ region.

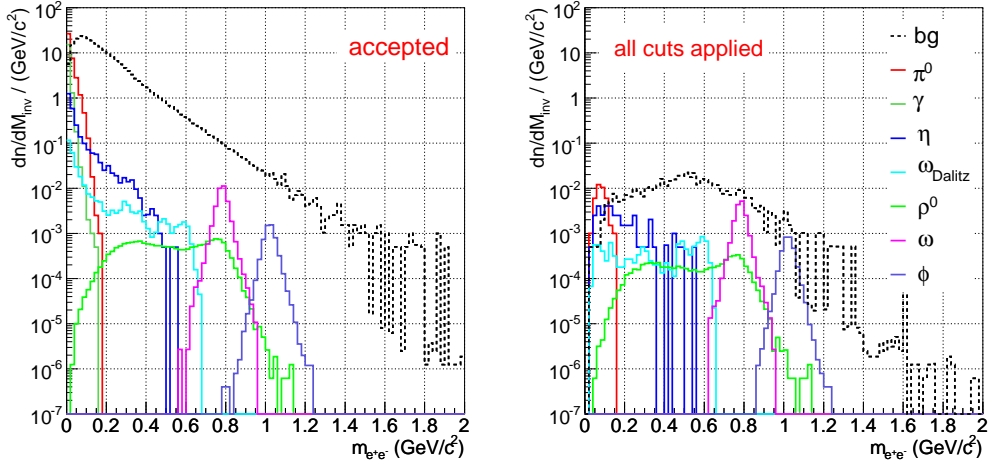


Figure 14: Invariant mass spectra before (left) and after (right) all cuts. Red: π^0 -Dalitz, dark green: γ , dark blue: η -Dalitz, blue: ω -Dalitz, magenta: ω , green: ρ^0 , violet: ϕ , black: combinatorial background.

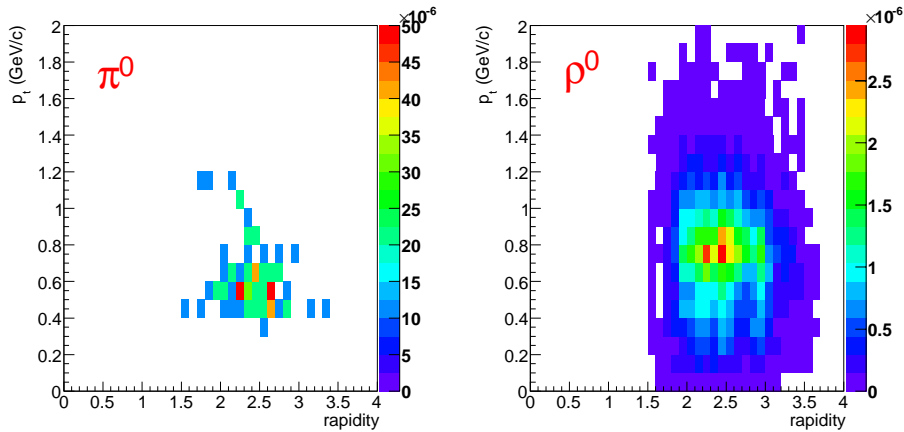


Figure 15: Transverse momentum versus rapidity distribution for π^0 -Dalitz decay (left panel) and for ρ^0 (right panel) after all cuts

The most effective cut to reduce background in the enhancement region (i.e. $0.2 < m_{e^+e^-}/(\text{GeV}/c^2) < 0.6$) is on the single track transverse momentum (p_t). It should be noted however, that this cut at the same time removes a substantial part of the π -Dalitz contribution. The final decision on whether to place this cut will also be driven by the physics focus on the pair spectrum. In contrast, the opening angle cut does not effect the background contribution in the enhancement region although more than 80% of the Dalitz-pairs

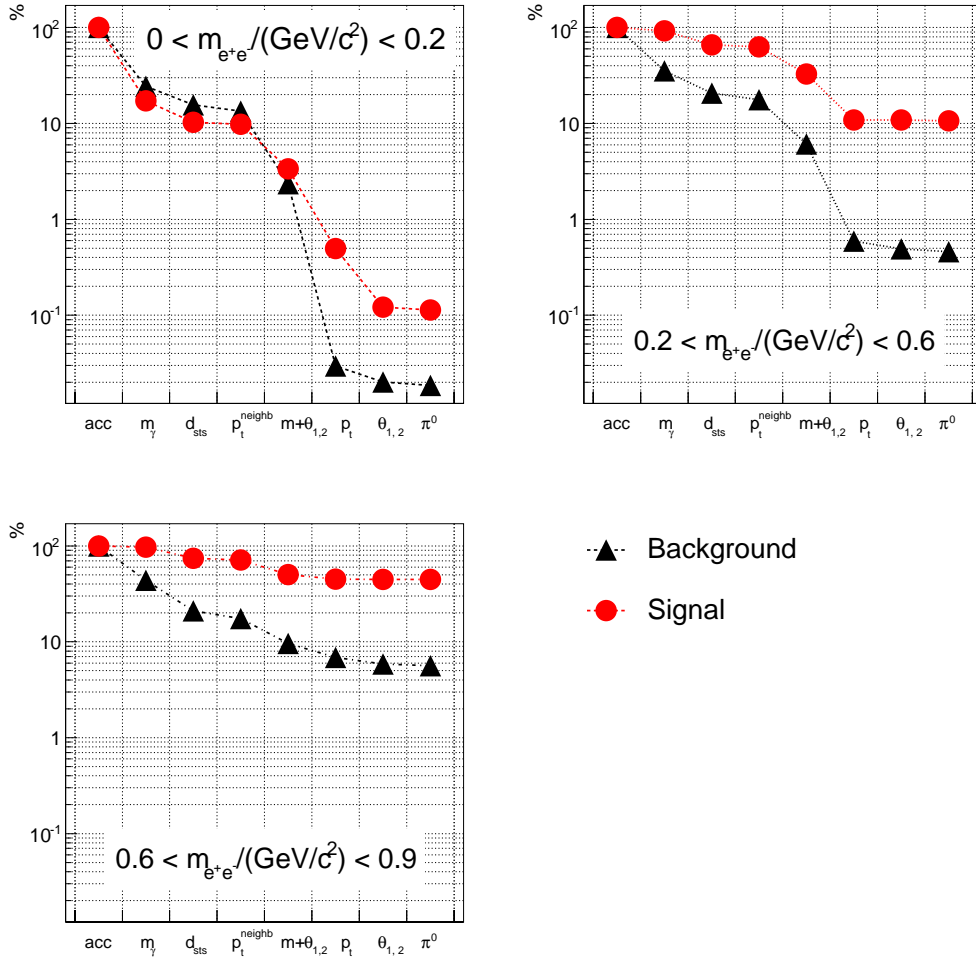


Figure 16: Cut efficiency. Red points: signal, black triangle: background in different mass region. Note that pairs from γ conversion are signal.

are removed. This observation needs further investigation.

The systematics of the signal-to-background ratio is shown in Figure 17. In the vector meson mass region, the signal-to-background steadily increases with each cut applied. At this level of background rejection, the maximum of the omega peak is just touching the combinatorial background. The integrals are given in Table 3. The ω and ϕ signal are visible above the combinatorial background (see Figure 18). The signal-to-background ratio in a $\pm 1.4 \sigma_m$ range around the vector meson peaks are about 0.5 for ω and 0.3 for ϕ , for π^0 -Dalitz the signal-to-background is about 2. In Figure 19, finally, we present the transverse momentum versus invariant mass distributions for correlated pairs after all cuts. In the right panel, the related reconstruction efficiency

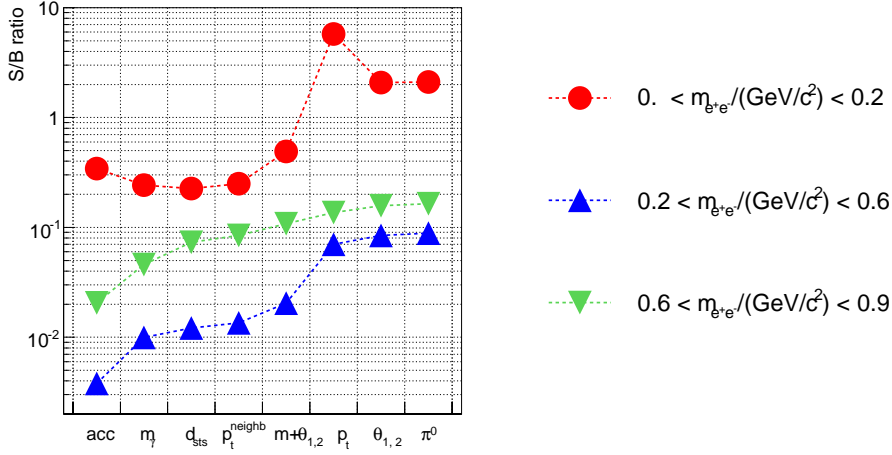


Figure 17: Signal-to-background ratio

mass region GeV/c ²	S/B ratio	
	accepted	after all cuts
0 ÷ 0.2	1/ 3	1/ 0.5
0.2 ÷ 0.6	1/ 267	1/ 11
0.6 ÷ 0.9	1/ 48	1/ 6

Table 3: Signal-to-background ratio

is depicted for 5 pair p_t bins.

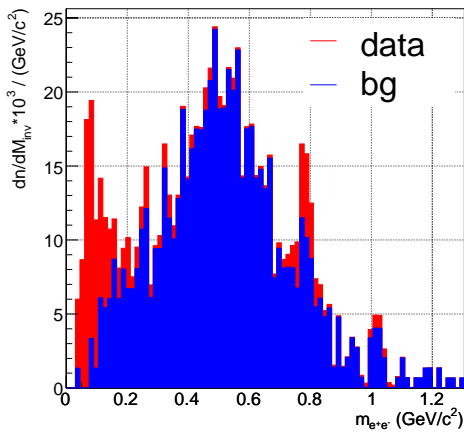


Figure 18: Invariant mass distribution. Red: all e^+e^- combinations (data), blue: combinatorial background (bg).

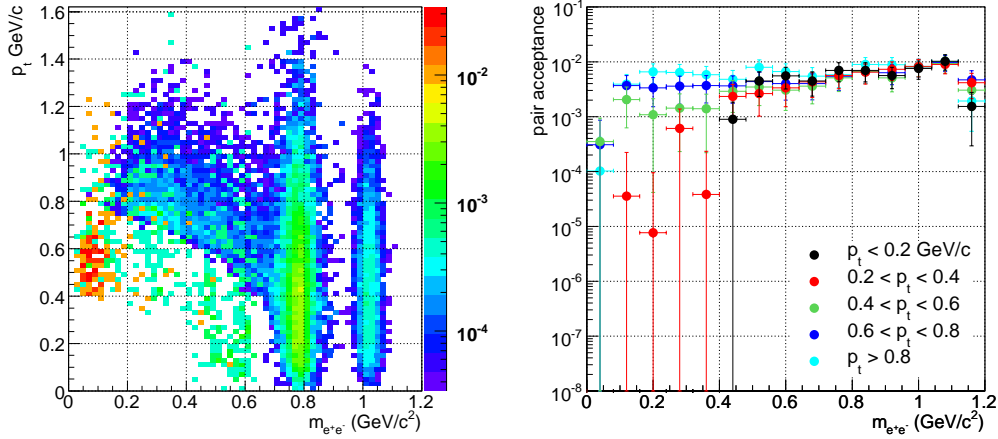


Figure 19: (Left panel) Distribution of accepted e^+e^- pairs in transverse momentum and invariant mass after all cuts. (Right panel) Pair acceptance as a function of invariant mass for different pair p_t .

6 Conclusions

We have presented results for low-mass electron pair reconstruction in central $Au + Au$ collisions at 25 AGeV. In the enhancement region ($0.2 < m_{e^+e^-}/(\text{GeV}/c^2) < 0.6$) the signal-to-background ratio is 1/11. This result could be improved by exploiting additional cuts like e.g. on the energy loss information in the tracking stations or by modifying the configuration of the tracking station. This first investigation of the background situation in the CBM experiment shows that it seems feasible to do low-mass electron pair spectroscopy. A full assessment of the situation, however, requires a full simulation including the detector responses. The next steps are:

- realistic simulation including track reconstruction, electron identification, momentum resolution;
- combinatorial background estimation using same-event or mixed-event techniques.

References

- [1] CERES Collaboration. *Low-mass e^+e^- production in 158 AGeV Pb-Au collisions at the CERN SPS, its dependence on multiplicity and transverse momentum*. arXiv:nucl-ex/9712008 v1 23Dec 1997.

- [2] S. Damjanovic on behalf of the NA60 Collaboration. *First measurement of the ρ spectral function in high-energy nuclear collisions*. Quark Matter 2005 proceedings, to be published in Nucl. Phys. A (nucl-ex/0510044).
- [3] R.J. Porter et al. [DLS Collaboration]. *Phys. Rev. Lett.* 79 (1997) 1229.
- [4] R. Holzmann for the HADES Collaboration. *Di-electron mass spectrum in 2 AGeV C+C measured with HADES*. Quark Matter 2005 proceedings, to be published in Nucl. Phys. A.
- [5] G.E. Brown and M. Rho. *Chiral restoration in hot and/or dense matter*. Phys. Rept. 269, 333 (1996), hep-ph/9504250.
- [6] R. Rapp and J. Wambach. *Chiral symmetry restoration and dileptons in relativistic heavy-ion collisions*. Adv. Nucl. Phys. 25 (2000) 1, hep-ph/9909229.
- [7] CBM collaboration. (2005, January). *Technical Status Report CBM Experiment*, 408.
- [8] S.A. Bass et al. (1998). *Prog. Part. Nucl. Phys.*, 225-370.
- [9] <http://www-hades.gsi.de/computing/pluto/html/PlutoIndex.html>
- [10] W. Cassing, E.L. Bratkovskaya. *Phys. Reports* 308 (1999) 65.
- [11] <http://wwwasd.web.cern.ch/wwwasd/>.
- [12] <http://www-cbm.gsi.de/cgi-bin/cvsweb/proto/cbmroot/geometry>
- [13] W. Peters, M. Post, H. Lenske, S. Leupold and U. Mosel, *The spectral function of the rho meson in nuclear matter*. Nucl. Phys. A **632** (1998) 109 [arXiv:nucl-th/9708004].